Microwave Plasmas Applied for Synthesis of Advanced Free-Standing Carbon Nanostructures

Luís Silva[1]

[1] MEFT/IPFN, Instituto Superior Técnico, Universidade de Lisboa, Lisboa, Portugal

E-mail: luis_silv@live.com

Abstract

Direct and selective synthesis of free-standing carbon nanostructures, including nanodiamonds and N-graphene, i.e. nitrogen-doped graphene, in a controllable manner, was achieved by the injection of nitrogen/carbon precursors into an argon microwave-induced plasma, driven by surface waves and kept at atmospheric pressure conditions. The single-step and selective synthesis of the nanostructures are achieved by externally controlling a few parameters, like the precursor and background gas fluxes, the microwave power and the relative ratio between the precursor's fluxes. Nanodiamonds synthesis was achieved using CO2/CH4 as carbon precursors, an argon flux of 2000 sccm and a microwave power of 1 kW. Synthesis of N-graphene was accomplished with a solution of ammonia in ethanol (4 wt %), with an argon flux of 1200 sccm and a microwave power of 2 kW. In the case of N-graphene, IR and UV irradiation were further applied on the post-discharge zone, to the flow of nanostructures to improve both the quality (sp2/sp3 ratio) and the purity, by effectively breaking the oxygen-carbon bondings and providing the thermodynamic conditions for the sheet growth. The samples were submitted morphological, structural, chemical and vibrational characterization methods using HRTEM, SEM, XRD, XPS and Raman spectroscopy. The plasma high-energy density environment was characterized by OES and the outlet plasma gas by FT-IR. N-graphene with a doping level of ~0.5% and nanodiamonds with hexagonal structure were synthesized.

Keywords: N-Graphene; Nanodiamonds; Microwave-Induced Plasmas; Direct synthesis; Free-standing material

1. Introduction and State of the Art

Carbon [1], the 6th element in the periodic table, is one of the most abundant elements in the Universe and has an essential role on Earth's ecosystem: it is part of all organic molecules, essential to all living beings. This results from the incredible versatility of the carbon atom when forming chemical bonds, where the s and p orbitals tend to overlap, hybridizing in sp, sp^2 and sp^3 orbitals. Thus, carbon can bond with other elements in many ways, resulting in a vast list of different chemical compounds. Even when it bonds with itself (carbon allotropes), carbon generates very distinctive substances, including diamond (sp^3), graphite (sp^2), carbines (sp), etc. In the 20th-century, the technological advances led to the development of new carbon-based materials, the carbon nanostructures [2], synthesized in the laboratory. Those materials showed new and improved properties bringing numerous application prospects. Some examples are the carbon nanofibers, highly-oriented pyrolytic graphite (HOPG), nanodiamonds (NDs), fullerenes, carbon nanotubes and finally graphene.

From the list above, NDs and graphene have been two of the most "eye-catching" materials, for their outstanding physio-chemical properties. Graphene [3], a flat monolayer of carbon atoms tightly packed into a two-dimensional honeycomb lattice, was presumed not to exist in the free-state since Landau and Peierls showed that the growth of strictly 2D crystals was thermodynamically unstable [4]. However, the path taken by Andre Geim and Konstantin Novoselov was not to synthesize it using a "bottom-up" approach but to isolate it, starting from graphite powder, using the so-called "scotch tape method". The subsequent experimental characterization of graphene's physical properties granted them the Nobel Prize in 2010 [5]. The ND particles, on the other hand, have an older history [6]. In 1961, DeCarli and Poulter Laboratories began experiments with graphite under shock waves which resulted

*

in the synthesis of sub-micron diamond crystals [7]. Almost at the same time, in 1963, in the old USSR, experiments with explosive charges, in controlled environments, resulted in the synthesis of ND particles as small as 2 nm. Furthermore, they were also detected in meteorites [8], dated back to the prehistory of the solar system, in the protoplanetary disks of new-born stars and synthesized in the form of films, an investigation work conducted by Gruen at the Argonne National Laboratory [9].

Plasmas are widely recognized for their applicability across many branches of science and technology, including the material science branch [10]. Due to their inner characteristics, plasmas revealed to be a useful nanofabrication tool; they comprise both thermal and chemical reactor function as well as catalytic properties, providing simultaneously high temperature and fluxes of excited atomic and molecular species, ions, electrons and high energy photons, leading to many different assembly pathways.

The goal of this work is indeed the application of a microwave plasma torch, a type of low-temperature non-equilibrium plasma, driven by surface waves at atmospheric pressure, to the direct synthesis of different carbon nanostructures, including nanodiamonds and nitrogen-doped graphene (N-graphene). The method is based on the use of different precursors of carbon and nitrogen in gas and liquid forms, that are injected in the plasma environment, being subsequently decomposed into simpler molecules and atoms. The complex chemistry between the different species, flowing downwards, leads to the nucleation of the solid carbon nanostructures in the post-discharge region, where the temperature drops. Despite being a complex process, the synthesis of the different structures can be effectively controlled by a set of few parameters such as the type of precursors employed and their relative fluxes, the background gas flux and the microwave power used to maintain the plasma. The modification of the background gas flux and microwave power supplied influences the plasma parameters such as the gas temperature and electron density, which combined with the modification of the precursor's fluxes ratio changes the assembly routes. In this work, it is demonstrated, the synthesis of nanodiamonds and graphene sheets doped with nitrogen. Furthermore, to optimize the N-graphene synthesis, it was applied both IR and soft UV irradiation in the assembly zone. The IR irradiation works as a heat source keeping the reactor's wall at a constant temperature. Previous works have shown that this extra heat promotes the growth of graphene sheets by influencing the thermodynamic conditions [47]. The application of UV radiation has the purpose to lower the sheet's oxygen level by "kicking off" the epoxy oxygen groups and other sp^3 carbons. The joint effect of UV and IR irradiation increased both the sheet's purity and quality, an effect observed on the ratio sp^2/sp^3_{all}.

1.1 Nanodiamonds

Nanodiamond [11, 12] is a term widely used in the literature to describe diamond particles with dimensions ranging from few to several hundred nanometres and diamond films with nanometric grain sizes. At the nanoscale, ND particles conserve most of the diamond's superior properties [13], such as the extraordinary mechanical hardness (Young and Bulk modulus), high thermal conductivity, chemical inertness and biocompatibility. However, due to their nano-size, the particle's surface properties also enter into play, influencing the particle's stability [12, 13]. In the nano-carbon phase diagram, the cluster size must be included as another parameter, as the contribution of the surface energy to the Gibbs free energy grows with the reduction of the cluster size. The inclusion of this extra parameter influences the thermodynamic conditions on the formation of sp^2 and sp^3 carbon, predicting a reversion of roles on their stability relatively to the macroscopic scenario. Indeed, for cluster sizes under 5 nm, first-principle calculations have shown that hydrocarbons (sp^3 carbon) are more stable than poly-aromatic rings (sp^2 carbon) [14]. With different morphologies and particles sizes, different surfaces become thermodynamically favourable [13]. For instance, ND particles can have graphitic-like reconstructed surfaces, terminated with different functional groups from oxygen, hydrogen, nitrogen, etc. Even the sp^2 type surfaces have their own chemistry. Due to their diamond core, stable and chemical inert, and a reactive surface nanodiamonds are envisioned for biomedical applications [15], such as bioimaging (fluorescence capability) [16], drug delivery, protein mimic and even for tissue scaffold [13].

Nanodiamond particles can be synthesized by several methods [12]. The most common ones are detonation synthesis [17], ball milling of high-pressure and high-temperature (HPHT) diamond [18-20] and laser pulsed ablation (LPA) [21-22]. Other lesser-known methods are ultrasound cavitation [23] and high-energy particle irradiation of graphite and carbon onions with both electrons and ions [24 – 26]. Only detonation synthesis, HPHT and LPA NDs are commercialized [27]. Detonation synthesis of ND particles involves the use of high-energy explosives (RDX and/or TNT) in the presence (or not) of a carbon precursor, enclosed in a chamber where the explosion occurs. The product, called detonation soot, is a composition of aggregates of primary ND particles with an average size of 5 nm, mixed with sp^2 carbon and metallic impurities. Although detonation synthesis represents the "front-line" in the large-scale production of NDs, it requires extensive post-synthesis treatments with hazardous chemicals to etch the sp^2 phase, remove the trapped impurities in the particle's aggregates and de-aggregate the primary-particles clusters. This is accomplished by using hazardous chemicals and expensive treatments. HPHT NDs are the main source of fluorescent NDs, due to the natural doping with nitrogen during the HPHT growth of diamond

*

particles. However, due to the extreme conditions needed, this method is more expensive than detonation synthesis. Other disadvantages include the contamination of the final product due to the milling agents used and its two-step nature. The milling step usually involves ceramic beads and ultrasonication, that can 'break' the particles to sizes from 10-20 nm, mono- or polycrystalline. PLA is based on the use of solid targets, commonly graphite, immersed in liquid media (benzene, water, etc.), where the laser is focused. The main advantages of PLA are its one-step nature and the synthesis of ND particles without introducing contaminants and agglomeration. Nevertheless, the costs are high, due to the high-power lasers used, and the yield is much lower when compared to the other methods.

Plasma-based methods for ND synthesis are almost resumed to plasma-enhanced chemical vapour deposition (PE-CVD), a technique employed on the synthesis of diamond films [28]. However, a few works reported the synthesis of ND powder in free-standing form using microwave-plasma torches [29-33]. These methods have been considered to be CVD-like methods in the literature. A recent work [33] describes the synthesis of diamond polymorphs (cubic-, n- and hexagonal-diamond phases) through the decomposition of ethanol in a microplasma environment. However, the few NDs that can be observed are among many other carbon allotropes (e.g. nanospheres of carbon, graphene, etc.) as evidenced by the Raman and XPS results.

1.2 N-graphene

Graphene [34,35], beyond its unique properties, can be used as an atomic scaffold from which other 2D materials can be formed through its doping [36]. Nitrogen, by being its neighbour element in the periodic table and thus having a similar radius, is a strong candidate for substitutional doping. When inserted in graphene's scaffold, nitrogen usually assumes three main configurations: quaternary-N, pyridinic-N and pyrrolic-N. In quaternary-N, a carbon atom gets replaced by a nitrogen. Pyridinic-N is a configuration where the nitrogen bonds with the carbons in a hexagon, and pyrrolic-N in a pentagon. Both configurations happen either at the sheet's edge or next to intra-sheet defects. The nitrogen doping of graphene can influence its electronic properties, by opening a bandgap (either n- and p-doping are possible) and its electrochemical properties, by creating active spots that can participate in ORR, without altering its original structure or graphene's properties [37].

These modifications in graphene's properties yield interesting applications prospects, namely its use in high-performance supercapacitors or batteries as an electrode [38, 39]. N-graphene synthesis methods list [40] includes direct and post-synthesis methods, being the difference in whether the doping step is conducted simultaneously or not with the synthesis of graphene. Direct methods include Chemical Vapor Deposition (CVD) [37], solvothermal synthesis [41] and arc-discharge [42]. CVD consists of growing N-graphene sheets on a substrate, usually, a silicon wafer coated with a metal catalyst, commonly nickel or copper, placed under a high-temperature atmosphere containing the carbon/nitrogen precursors. Gas, liquid and solid precursors can be used. The process offers some controllability on the nitrogen doping level and configuration (precursor's ratio, temperature, type o precursor, etc.). However, the synthesis conditions require the use of expensive equipment (vacuum pumps, expensive reactors), thus increasing the method's cost. An additional setback is the use of the substrate to grow the sheet, being needed etching methods to remove the N-graphene sheet, which can compromise the structure and introduce defects. The solvothermal method is reported as a scalable and easy method, however, the reaction uses hazardous chemicals and introduce contaminants to the final product. Another approach used to achieve graphene's doping is the use of post-treatment methods. These methods, by being two-step, are dependent on previous graphene synthesis. Usually, the employed method is chemical or thermal exfoliation of graphite, which yields as final product graphene-oxide (GO). Common post-synthesis methods include thermal annealing [43] and wet-chemical reaction (also known as hydrothermal method [44]). The first consists on submitting GO on high-temperature atmosphere, in the presence on N-precursors which simultaneously reduces and inserts the nitrogen atoms into graphene scaffold. The hydrothermal method uses acids to reduce GO and doping it with nitrogen. Both methods offer scalability and are relatively cheap, however, the obtained NG is usually contaminated with a high level of oxygen (typically above ~5%) which greatly compromises its electronic properties.

Plasma methods for N-graphene synthesis are almost summarised in plasma treatment of graphene [45,46], or employed in CVD. A niche and barely known application of plasmas as a direct method have been described in [47]. There, it was demonstrated the synthesis of graphene powder, composed of graphene nano-sheets with very high quality. The method has further been improved to include the direct doping of graphene by simply adding a nitrogen precursor to the plasma [48], a method improved and dein this work.

2. Experimental Methods

The experiments leading to the synthesis of the nanocarbon structures were conducted on a microwave plasma sustained by surface waves. The setup consists of a surfatron-waveguide type launcher coupled to a 2.45 GHz microwave generator (Sairem) through a waveguide (WR-340) system. The plasma reactor, a quartz tube, is inserted perpendicularly to the waveguide and is coupled to the power through the launcher. The background gas, argon, is being injected under laminar flow conditions. The precursors are delivered into the plasma region through a thinned concentric quartz tube.

*

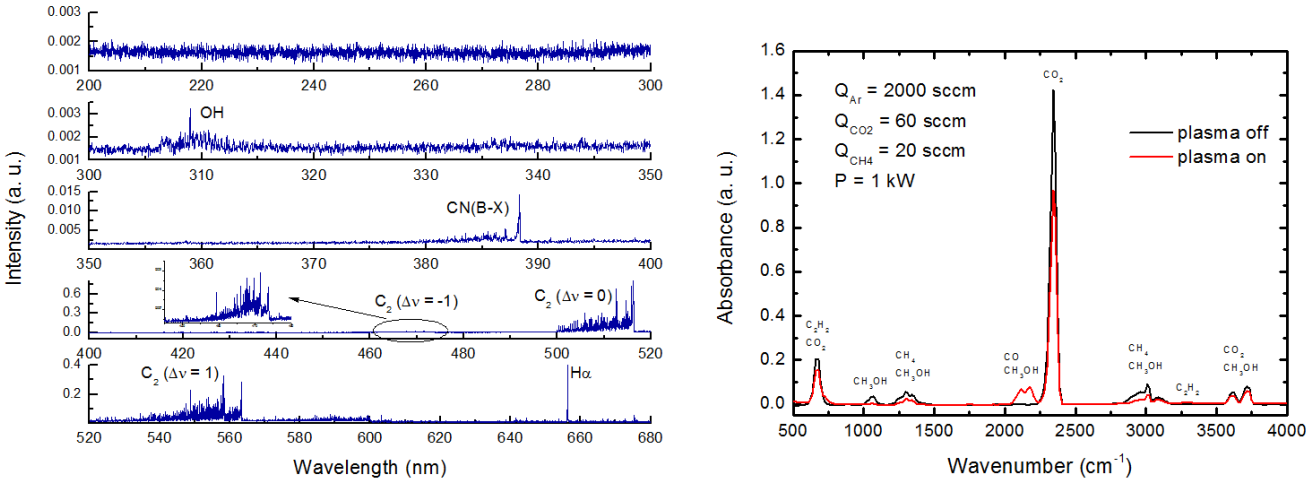

Figure 1 - (Left) OES spectrum from the region close the launcher, for the experimental conditions of sample ND2. (Right) FT-IR spectrum of the outlet gas stream with the plasma turned on and off, for the experimental conditions of sample ND1.

Nanodiamonds experiments were conducted using a constant microwave power of 1 kW and a background gas flux of 2000 sccm. Both were kept constant through all the experiments. Methane and carbon dioxide were used as carbon precursors, being the respective fluxes varied between 20-80 sccm and 20-60 sccm. The precursors were inserted into the in the plasma with their own tubes.

N-graphene experiments were conducted using a constant microwave power of 2 kW with the background gas flux varying from 1000 to 1500 sccm. Part of the background gas flow passes through a tank filled with the precursor, placed inside of a sonication bath, to drag the ethanol/ammonia (4 wt %) precursor. The precursor partial flux was varied in the range of 50 to 120 sccm for different background gas fluxes. Moreover, both IR and UV irradiation was applied to the nanostructures flux in the post-discharge region to increase improve both the quality and purity of the N-graphene structures. The system with a network of IR lamps (20 cm) is placed immediately after the end of the plasma zone (15-30 cm from the launcher). The wall temperature, an effect of the IR irradiation, was monitored with a FLIR thermal imager. The nanostructures were captured by a tornado type cyclone system followed by a water trap to capture the nanostructures able to escape with the gas flow. The N-graphene powder in a glass container was further irradiated with soft UV radiation, in the range 300-400 nm with a power of 4 W.

The specific details of the experimental scheme can be found elsewhere for both nanodiamond- and N-graphene experiments [49].

2.1 Plasma Characterization Techniques

To probe the different species in the plasma high-density environment, plasma emissions were collected by an optical fibre and directed to the entrance of a Jobin-Yvon Spex 1250 spectrometer (1200/2400 g/mm grating) equipped with a CCD camera, featuring a 13.5 µm pixel-size.

A portion of the output gas stream from the plasma reactor was directed to an FT-IR Thermo Nicolet 5700 spectrometer, functional in the range 0-7000 cm^{-1}, to measure the absorption spectra and identify the different substances that flow out with the solid nanostructures.

2.2 Material Characterization Techniques

The structures were subject to morphological, structural and chemical characterizations by means of different diagnostics. Nanodiamond samples were analyzed using XRD, HRTEM/SEM and Raman spectroscopy. N-graphene samples were analyzed using XPS, SEM and Raman Spectroscopy.

Morphological analysis was conducted using SEM. The characterization of the samples has been performed using a JEOL, JSM-7001F field emission gun scanning electron microscope operating in secondary electron imaging mode (SEI) using 15 kV accelerating voltage. The samples were deposited on a double-sided carbon tape mounted on an aluminium stub. HRTEM was conducted by a Hitachi H8100 TEM using 200 kV accelerating voltage. Fast Fourier Transform (FFT) was applied to the regions where the crystalline structures were identified to determine the interatomic distance.

To probe the phonon structure of the nanostructures, and to provide a quick and easy structural and qualitative characterization of the samples Raman spectroscopy analysis was performed. The synthesized nanostructures were freely suspended on a glass substrate and the Raman spectra from different regions of the sample were obtained using a LabRAM HR Visible (Horiba Jobin-Yvon) Raman spectrometer with 1 cm^{-1} spectral resolution and 633 nm He-

*

Ne laser excitation with laser spot size of 2 μm. Measurements were performed with a laser power P_l = 0.054 mW to avoid overheating.

Free-standing N-doped graphene sheets were characterized by X-Ray photoelectron spectroscopy using an XSAM800 spectrometer from KRATOS with an incident X-radiation from an Mg Kα source (1253.6 eV). Operating conditions and spectra acquisition parameters are detailed elsewhere [2]. Fluffy powder samples were mounted on the XPS holder with a double face tape. No silicon was detected discarding any interference of the tape spectrum. No charge correction was needed, since the C 1s main peak, detected at 284.4 ± 0.1 eV, is typical of aromatic C-C or C-H in graphene. The sensitivity factors (from Vision 2 library) used for quantification purposes were 0.318 for C 1s, 0.736 for O 1s and 0.505 for N 1s.

3. Results and Discussion

3.1 Nanodiamonds

From the several ND experiments made, only two relevant samples were chosen for result analysis. These samples are representative of how the variation of the precursor's flux can modify the type of structures produced. Their experimental conditions are presented in Table 1.

Table 1 – Precursors fluxes used for synthesis of ND1 and ND2 samples.

Samples	Q_{CO2} (sccm)	Q_{CH4}(sccm)
ND1	60	20
ND2	20	40

3.1.1 Plasma Characterization

The emission spectrum of the $Ar/CO_2/CH_4$ plasma (Figure 1) in the range 200-680 nm was collected by OES immediately after the launcher (plasma hot region), to detect the products from the decomposition of the CO_2 and CH_4 in the plasma. The emission bands identified, corresponds to C_2 (Swan band system ($d^3\Pi_g \rightarrow a^3\Pi_u$) between 450-570 nm) where the transitions Δv = -1,0,1 are visible, to CN (violet system ($B^2\Sigma^+ \rightarrow X^2\Sigma^+$) between 350-420 nm) and to OH (Q_1 branch between 307.5-315 nm). Furthermore, the atomic line belonging to the hydrogen (Balmer-alpha line H_α (656.3 nm)), is also observable in the spectrum. From the emission spectrum is clear that the carbon dimer (C_2) dominates the emissions close to the launcher which explains the typical green colour of the plasma. That emission is caused by the radiative decay of the $C_2^*(A^3\Pi_g)$ state. Moreover, the plasma temperature was estimated using the OH Q_1 branch to calculate its rotational temperature, using the Boltzmann plot method [50]. The rotational temperature of the OH radical, in atmospheric pressure plasmas, can be assumed to be equal to the gas temperature under a local thermodynamic equilibrium assumption [51]. This assumption relies on the high collision rates expected for these plasmas kept at atmospheric pressure. The gas temperature estimated was T ≈ 2100 K (experimental conditions of sample ND2).

FT-IR analysis of the outlet gas stream has been performed in the cases where the plasma was turned on and off. The spectrum was collected between 500 and 4000 cm^{-1} for the experimental conditions of the sample ND1. When the plasma was off, several spectra lines were detected, including the methane (CH_4), carbon dioxide (CO_2), water, acetylene (C_2H_2) and methanol (CH_3OH), which are products of the precursor's reaction without the plasma. With the plasma on, new lines appear while the existing ones – with the plasma off - decrease. The new lines correspond to new excited states of the already identified molecules being the novelty the line belonging to carbon monoxide (CO). Through the relative decrease in the absorbance of the detected bands, it was possible to infer a precursor's decomposition close to 50%.

3.1.2 Material Characterization

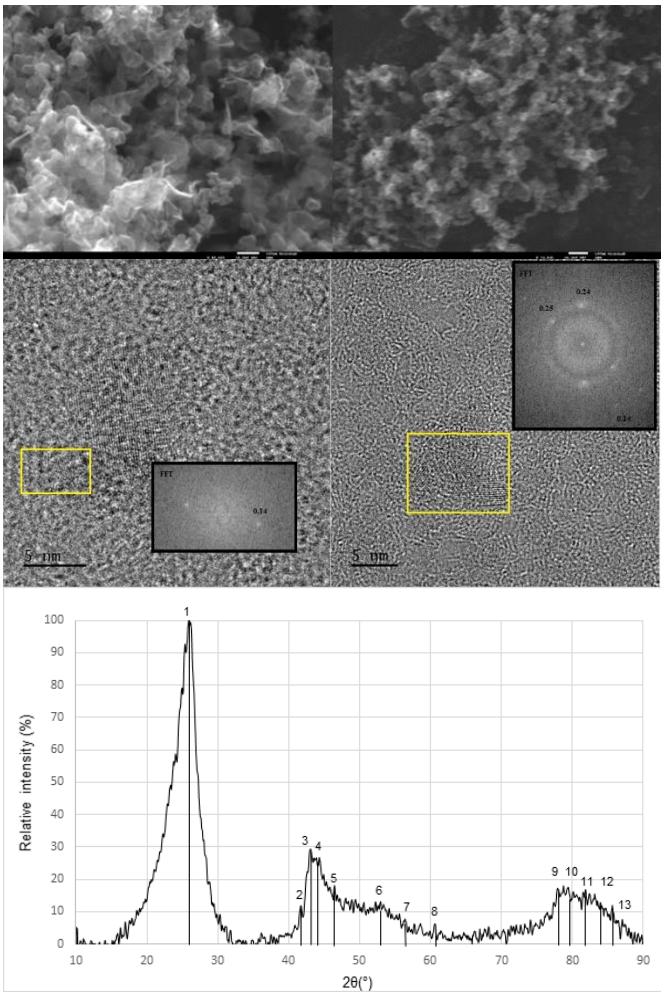

Figure 2 – (1st) SEM images of the samples ND1 (left) and ND2 (right). (2nd) HRTEM images of sample ND2. (3rd) XRD spectrum of sample ND2.

*

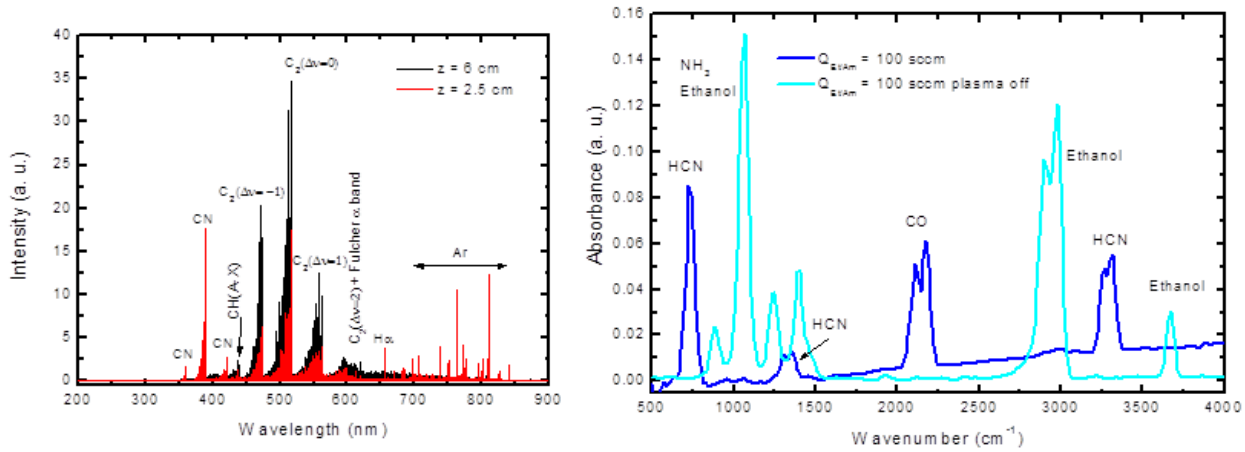

Figure 3 – (Left) OES spectrum from two different positions from the launcher (z = 2.5 and 6 cm). (Right) FT-IR spectrum of the outlet gas stream with the plasma turned on and off. Both spectra where taken for the experimental conditions of sample NG_3.

The ND samples were first characterized by SEM and their relative morphology compared. The SEM image corresponding to ND1 (Figure 2) shows the presence of graphene-like structures, identifiable by the smooth folded surfaces with curved edges. ND2, on its turn, shows the presence of particle-like structures, presenting a "cluster" character, which is usually the indication for the presence of ND particles, knowing their tendency to be formed in aggregates.

Following the indication taken from the SEM images, ND2 sample was submitted to XRD analysis. The spectrum (Figure 2) reveals the presence of different bands: the dominant graphitic peak (002) and two other bands for 2θ ϵ [40º, 60º] and [70º, 90º]. These two bands can be attributed to the presence of diamond phase in the sample; besides the graphite's (100) plane, other lines can be identified in the first region, the most relevant being caused by the planes (100) from 6H-diamond (Lonsdaleite [52]) and (200), a reflection commonly attributed to the n-diamond phase [53], a diamond polymorph derived from the cubic-diamond structure. In the second region, further reflections are found. It is to be noted that phase identification in crystallography from XRD spectra is an empirical process. Usually, the most intense reflections are found and associated with the corresponding phase. Based on that knowledge, the identification of the other less-intense reflections is conducted. For example, as graphite was clearly presence due to its first line, it is expected that the other less intense features should also be present. The same works for the 6H-/n-diamond phases. Furthermore, it was possible to identify the presence of the lines corresponding to the planes (110) of graphite, (110) of 6H-diamond and (220) from cubic-diamond (this line is common to both phases). Finally, the line corresponding to the (103) plane of the hexagonal phase was also identified.

These results were then crossed with HRTEM images of the sample ND2 (Figure 2). Although the interaction of the electron beam with the sample affected the resolution (reduction of the exposure time), crystalline structures were still identified, and the inter-atomic distance measured by means of the FFT of the regions showing organized crystalline structures. The identified structures have sizes under 10 nm and from the FFT results, it was possible to determine those distances of 0.14 nm, 0.2 nm and 0.34 nm. These distances can be crossed with the results of the XRD spectrum, which permits to attribute the 0.14 nm to the reflection (102) of the 6H-diamond.

The sample ND2 was further analysed with Raman spectroscopy, with three different laser wavelengths (458 nm, 515 nm and 633 nm). The spectra revealed the presence of the main band between 1000-1800 cm^{-1}, which can be further split in two peaks, the first centred about ~1350 cm^{-1} and the other about ~1600 cm^{-1}. The first peak showed a dispersive character, by blue shifting with the increase of the laser's wavelength. It is known, from the XRD results, that the well-known graphitic Raman features [54] must be present in the form of the G- and D-peaks (the D-peak also present a dispersive character). Further, its intensity must be reinforced due to the laser wavelengths used, which resonates strongly with the sp^2 carbon-phase in detriment of sp^3 carbon (by a factor of 50). These can be associated with the peaks fitted in the ranges 1580-1590 cm^{-1} and ~1330-1360 cm^{-1}, respectively. However, this spectrum is clearly different from the well-known graphite spectrum, which indicates the presence of other features. From the combined analysis of XRD/HRTEM, it was clearly demonstrated that crystalline diamond structures (6H-diamond) were present on the sample ND2. Thus, two extras features, about ~1170 cm^{-1} and ~1250 cm^{-1} were fitted within the band, based on previous results that showed that these peaks have been identified as characteristic features of the ND Raman spectrum, corresponding to trans-polyacetylene functional groups and derived from the phonon confinement model [55].

Concluding, the combined results of XRD and HRTEM permitted to clearly understand that, besides graphitic-like

*

structures, diamond structures were also synthesized. The results pointed strongly to the identification of the hexagonal-diamond phase, although the forbidden reflection belonging to the n-diamond was also present. HRTEM showed clearly the presence of crystalline structures with sizes under 10 nm and the measured inter-atomic distances, particularly 0.14 nm, can only correspond to the reflection (102), from the 6H-diamond phase. The results did not exclude, however, the possibility of the presence of other diamond polymorphs, namely n-diamond. From the Raman spectra, it was possible to understand that other structures different from graphitic-like structures were present on the sample, which by assuming that it could be NDs lead to biased fitting and consequently the identification of two of the several features present on ND Raman spectrum. The most important line, the diamond line at ~1330 cm^{-1} could not be identified, possibly because of the laser wavelengths used.

3.2 N-graphene

Table 2 – Atomic concentrations and atomic ratios of the NG samples.

Sample	NG_3	NG_4		
		-	IR (200 ºC)	IR (200º C) + UV
$Q_{Et/Am}$	100	120	120	120
C_C (%)	96.1	97.7	97.2	97.7
C_N (%)	0.48	0.22	0.16	0.44
C_O (%)	3.4	2.1	2.7	1.9
sp^2/sp^3_{all}	2.0	2.8	2.8	3.8

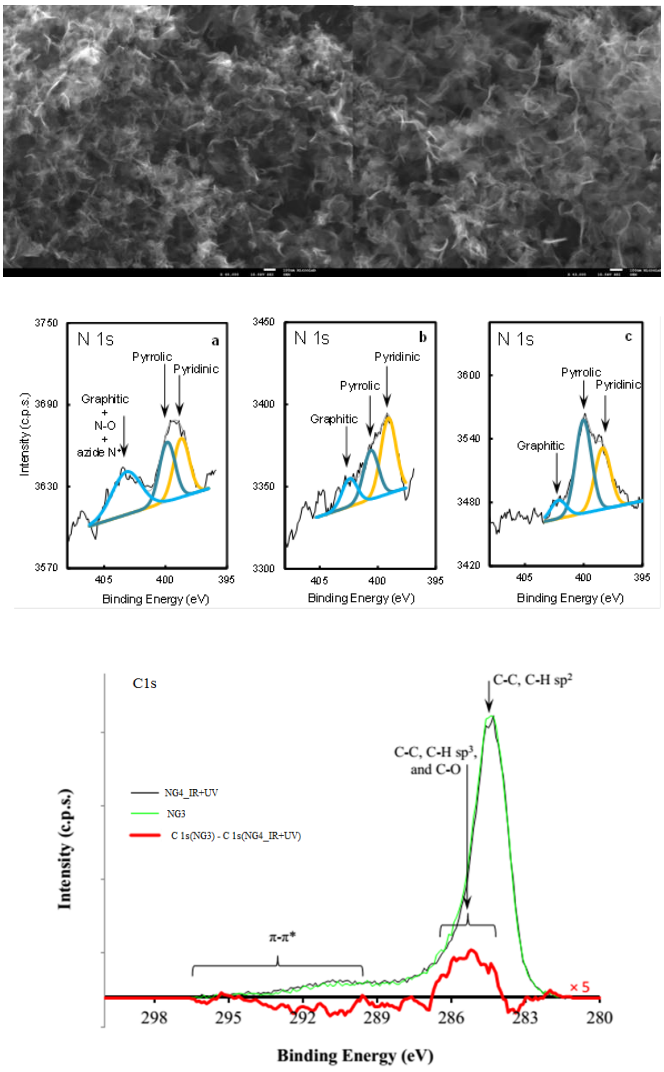

Figure 4 – (1st) SEM images from samples NG_3 (left) and NG_4_IR+UV (right). (2nd) Detailed XPS N1s regions of NG samples: a) NG_4; b) NG_4_IR; c) NG_4_IR+UV. (3rd) Comparison between the C1s peaks for the samples NG_3 (green) and NG_4_IR+UV (black).

3.2.1 Plasma Characterization

The visible emissions of the argon/ethanol/ammonia plasma in the range 200-900 nm were collected for two different axial positions inside the plasma hot zone (z = 2.5 cm and 6 cm) (Figure 3). From the measure spectrum it was possible to conclude that the plasma decomposes the ethanol/ammonia molecules in different molecular and atomic species based on the detection of CN (violet system ($B^2\Sigma^+ \rightarrow X^2\Sigma^+$) between 350-420 nm), C_2 (Swan band system ($d^3\Pi_g \rightarrow a^3\Pi_u$) between 450-570 nm), the radical OH (Q_1 branch between 307.5-315 nm) and the hydrogen Balmer-alpha line Hα. Furthermore, several atomic Ar lines are also observable in the spectrum. Note that the relative intensities of the detected bands vary with the position where the emission was collected. At z = 6 cm, away from the launcher, the emission spectrum is dominated by the C_2 molecules, a scenario different from what happens at z = 2.5 cm, closer to the launcher where the CN molecule emissions are dominant. This explains the colour transition from violet (close to the launcher) to green. The plasma gas temperature was estimated using the OH rotational spectrum corresponding to the Q_1 branch measured at z = 2.5 cm. The estimated temperature was T ≈ 3800 K.

The FT-IR spectrum (Figure 3) was taken between 500 and 4000 cm^{-1} with the plasma turned on and off. With the plasma off, the lines corresponding to the precursors, ammonia and ethanol the only ones detected. When the plasma is turned on, these lines disappear completely, being substituted by new lines corresponding to C_2H_2, HCN and CO revealing a total conversion of the precursors.

3.2.2 Material Characterization

NG samples were first analysed with XPS, which showed that nitrogen was present in all samples. Two fruitful analyses are between the samples with the highest doping level (NG_3

*

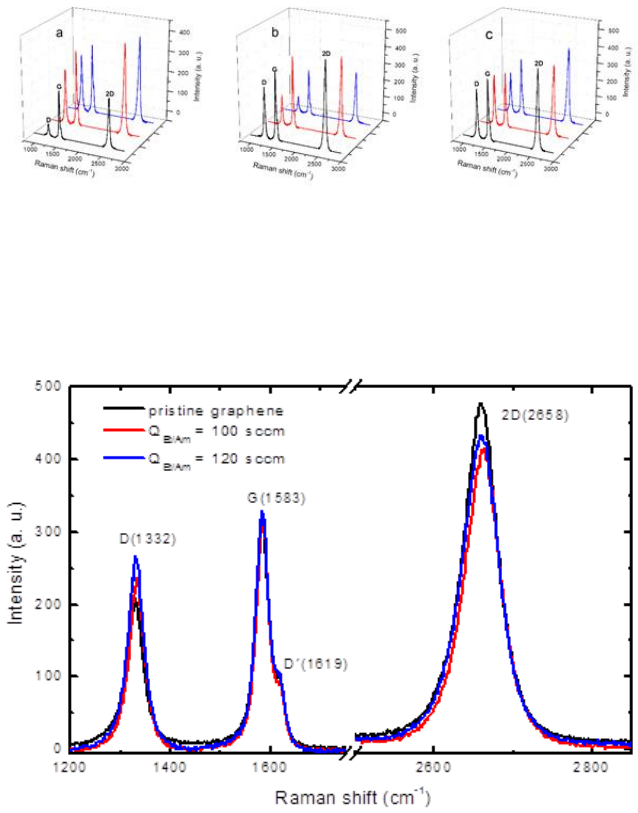

Figure 5 – (1st) 3D representation of the Raman spectrum taken from three different locations (sample NG_4). (2nd) Raman spectrum for pristine graphene and samples NG_3 and NG_4_IR+UV.

and NG_4_IR+UV) and the effects or IR and UV irradiation on the final product (NG_4 samples).

The detailed XPS binding regions detected at high resolution for the N1s peak for the samples NG_4, NG_4_IR and NG_4_IR+UV are shown in Figure 4. The N1s is fitted to the different contributions corresponding to the different nitrogen functional groups. In the N-graphene samples where additional heat (NG_4_IR and NG_4_IR+UV) was applied, three peaks centred at 398.7 eV, 400.2 eV and 402.3 eV are identified. These peaks can be attributed to pyridinic, pyrrolic and graphitic nitrogen, respectively. For the sample synthesized without additional heating (NG_4), there is an extra feature at 403.2 eV, which besides graphitic nitrogen can also include nitrogen bound to oxygen like nitroso groups. The C1s region shows a main peak centred at 284.4 eV, assigned to sp^2 carbon. Furthermore, other features assigned to sp^3 carbon bonds with other carbons, hydrogen and oxygen can be seen in the region 285-289 eV. The characteristic π-π^* excitations shifted to slightly higher binding energies are also present. Another meaningful feature is the C KLL Auger regions and their first derivatives, which can confirm strong electron delocalization of these carbon structures, a graphene's defining feature. From the first derivative, a characteristic parameter, the D parameter, which represents the energy difference between two consecutive extremes can be extracted. In this case, the measured D parameter was 20.6 eV, which is close to that of graphite. It is interesting to notice that samples NG_4 and NG_4_IR+UV, that are less oxidized and have more nitrogen than NG_4_IR, show a relative maximum at ~260 eV in the Auger fine structure of dN/dE that is absent on NG_4_IR. This small difference can be related to the different local density of the valence states which depend on the chemisorbed species.

A direct comparison between the samples NG_3 and NG_4_IR+UV was made. These samples possess similar doping level, but NG_3 possess a higher oxygen level than NG_4_IR+UV. The difference between their C1s regions is shown in Figure 4. Prior to the subtraction, the background was subtracted and the main peak of NG_3 was normalized to the maximum of NG_4_IR+UV to highlight the less intense spectral features: the positive peak shows that NG_3 has more sp^3 carbon than NG_4_IR+UV and the slightly negative "band" in the region of the π-π^* excitations shows that NG_3 has less delocalized electrons than NG_4_IR+UV, pushing it further away from graphene structure. This is a clear evidence that the extra IR+UV irradiation reduced the oxygen by breaking the bonds between the carbon and the oxygen atoms and "restored" the graphene's π-system. The SEM images of both samples reveal the inherent characteristics for the graphene morphology, i.e., the smooth folded surfaces with curved edges (brighter regions). The curly and smooth features are observed on both images, are an indication that the graphene structure is retained after the doping.

The Raman spectra of the NG samples with the highest doping level (NG_3 and NG_4_IR+UV) are shown in Figure 5. All three spectra show three dominant peaks at about 1332 cm^{-1}, 1583 cm^{-1} and 2658 cm^{-1}, attributed to D-, G- and 2D-peak, respectively. The effect of the nitrogen doping can be seen in the increase of the intensity of the D-peak and a decrease in the 2D-band, measurable in the ratio of both peaks. While in pristine graphene the intensity ratio (2D/G) is 1.5, in the case of both N-graphene samples, NG_3 and NG_4_IR+UV, the ratio decreases, respectively to 1.3 and 1.28. This ratio is still high enough to conclude that the synthesized structures are still graphene, but in the present case with defects induced by the nitrogen doping. Finally, to compare the doping homogeneity of the different NG_4 samples, the Raman spectra taken from three different locations in each sample are shown in Figure 5. The sample NG_4 (without the application of IR and UV) shows a strong variation in the D/G ratio, from 0.26 to 0.83, while the intensity ratio of the 2D/G varies from 1 to 1-2. A similar behaviour is observed for the NG_4_IR sample. From these results, it can be concluded that the defects are not homogeneously distributed. However, in the sample NG_4_IR+UV, an increase of the D/G ratio up to 0.9 is

*

observed. This ratio is nearly constant for the three different locations on the NG sample. It seems that more homogeneous distribution of defects, in particular, N-doping, of graphene scaffold is achieved by applying both heat and UV irradiation.

Concluding, direct doping of graphene sheets with nitrogen was successfully achieved through this plasma method. SEM images and Raman spectra show that the graphene structure is retained after doping and that the doping effect is visible through the increase of defects. XPS and Raman showed that the application of UV and IR to the structures resulted in a better sheet quality translated by the increase of the sp^2/sp^3 ratio and reduction in the oxygen level and a more homogeneous distribution of defects.

4. Conclusions and Final Remarks

By using a microwave plasma-based method, direct synthesis of ND particles with sizes from 2-10 nm, possessing hexagonal crystalline structure and N-graphene nanoflakes (100-500 nm) with a level of nitrogen doping ~0.5% was achieved. Nanodiamonds were synthesized by using carbon dioxide and methane as carbon precursors whereas N-graphene has been obtained using a solution of ammonia in ethanol (4 wt %) as carbon and nitrogen precursors. The selective synthesis was achieved by using different precursors and changing the plasma parameters (gas temperature, electron density, etc.) through the background gas flux and the microwave power supplied. Further, within each experiment, to optimize the synthesis process, the ratio of the precursors was changed. By changing the precursor's fluxes, it was possible to modify the chemical equilibrium within the system and thus change the assembly paths. In the case of N-graphene, the irradiation with IR and UV light was used in the post-discharge zone of the plasma where the structures assemble, to increase the sp^2/sp^3_{all} ratio. The extra heat supplied by the IR irradiation modified the thermodynamic equilibrium toward the assembling of sp^2 carbon instead of sp^3 carbon. The effect of the UV irradiation could be seen in the decrease of the level of oxygen detected (by XPS) in the samples irradiated (<2%) and consequently in the reduction of the sp^3 bonds between carbon and oxygen, whose effect was translated in the increase of the ratio sp^2/sp^3_{all}.

Acknowledgements

This work was realized partially under the project PEGASUS (Horizon 2020 FET-OPEN Grant number 766894). Considering the results analysis, namely the XRD/HRTEM and the XPS, I would like to thank to professor Amélia Rego and doctor Ana Ferraria for the help in the data analysis and interpretation. Finally, considering all the plasma experiments conducted for sample production, I thank to doctor Neli Bundaleska for the guidance and orientation through all the work.

References

[1] Royal Society of Chemistry. Royal Society of Chemistry. Periodic Table. [Online] 2018. http://www.rsc.org/periodic-table/element/6/carbon.

[2] Dresselhaus, M. S., Dresselhaus, G. and Eklund, P. C. Science of Fullerenes and Carbon Nanotubes. s.l. : Academic Press, 1996.

[3] Electric Field Effect in Atomically Thin Carbon Films. Novoselov, K S, et al. 2004, Science, Vol. 306, pp. 666-669.

[4] The structure of suspended graphene sheets. Meyer, Jannik C, et al. 2007, Nature, Vol. 446, pp. 60-63.

[5] Graphene prehistory. Geim, A. K. 2012, Physica Scripta.

[6] On the history of the discovery of nanodiamond synthesis. Danilenko, V V. 2004, Physics of the Solid State, Vol. 46, pp. 595-599.

[7] Formation of Diamond by Explosive Shock. DeCarli, P. S. and Jamieson, J. C. 1961, Science, Vol. 133, pp. 1821-1822.

[8] Vul, Alexander Ya. and Sherendova, Olga A. Detonation Nanodiamonds: Science and Applications. s.l. : Pan Stanford Publishing, 2013.

[9] NANOCRYSTALLINE DIAMOND FILMS. Gruen, Dieter M. 1999, Annual Reviews Material Science.

[10] Plasmas for environmental issues: From hydrogen production to 2D materials assembly. Tatarova, E., et al. 2014, Plasma Sources Science and Technology, Vol. 23.

[11] Shenderova, Olga A. and Gruen, Dieter M. Ultrananocrystalline Diamond: Synthesis, Properties, and Applications. 1º. s.l. : William Andrew Publishing, 2006.

[12] —. Ultrananocrystalline Diamond: Synthesis, Properties, and Applications. 2º. s.l. : Elsevier, 2012.

[13] The properties and applications of nanodiamonds. Mochalin, Vadym N, et al. 2011, Nature Nanotechnology, Vol. 7, pp. 11-23.

[14] Nanometre-sized diamonds are more stable than graphite. Badziag, P., et al. 1990, Nature, Vol. 343, pp. 244-245.

[15] Biomedical applications of nanodiamond (Review). Turcheniuk, K and Mochalin, Vadym N. 2017, Nanotechnology, Vol. 28.

[16] Improving surface and defect center chemistry of fluorescent nanodiamonds for imaging purposes — a review. Nagl, Andreas, Hemelaar, Simon Robert and Schirhagl, Romana. 2015, pp. 7521-7536.

[17] Detonation-synthesis nanodiamonds : synthesis , structure , properties and applications. Dolmatov, V Yu. 2007, Russian Chemical Reviews, Vol. 339, pp. 339-360.

[18] High yield fabrication of fluorescent nanodiamonds. Boudou, Jean-paul, et al. 2009, Nanotechnology, Vol. 20.

[19] Synthesis of diamond from carbon nanotubes under high pressure and high temperature. Cao, Limin, et al. 2001, Carbon, Vol. 39, pp. 311-314.

[20] Conversion of fullerenes to diamond under high pressure and high temperature Conversion of fullerenes to diamond under high pressure and high temperature. Ma, Yanzhang, et al. Applied Physics Letters, Vol. 65.

[21] Laser ablation in liquids : Applications in the synthesis of nanocrystals. Yang, G W. 2007, Progress in Materials Science, Vol. 52, pp. 648-698.

[22] Origin of the nano-carbon allotropes in Pulsed Laser Ablation in Liquids synthesis synthesis. Amans, David, et al. 2016, Journal of Colloid And Interface Science.

*

[23] Experimental Corroboration of the Synthesis of Diamond in the Cavitation Process. Galimov, M, et al. 2004, Doklady Physics, Vol. 49, pp. 150-153.

[24] Production of nanodiamonds by high-energy ion irradiation of graphite at room temperature. Daulton, T L, et al. 2001, Nuclear Instruments and Methods in Physics Research B, Vol. 177, pp. 12-20.

[25] Formation of diamond in carbon onions under MeV ion irradiation Formation of diamond in carbon onions under MeV ion irradiation. Wesolowski, P, et al. 2012, Applied Physics Letters, Vol. 1948, pp. 6-9.

[26] Carbon Onions as Nanoscopic Pressure Cells for Diamond Formation. Banhart, F. and Ajayan, P. M. 1996, Nature, Vol. 383.

[27] Currently Available Methods of Industrial Nanodiamond Synthesis. Dolmatov, V Yu, et al. 2004, Physics of the Solid State, Vol. 46, pp. 611-615.

[28] Microstructure of ultrananocrystalline diamond films grown by microwave Ar-CH4 plasma chemical vapor deposition with or without added H2. Jiao, S., et al. 2001, Journal of Applied Physics, Vol. 90, pp. 118-122.

[29] Homogeneous nucleation of diamond powder in the gas phase. Frenklach, M., et al. 1989, Journal of Applied Physics, Vol. 66, pp. 395-399.

[30] Synthesis of diamond powder in acetylene oxygen plasma. Howard, W, et al. 1990, Journal of Applied Physics, Vol. 68, pp. 1247-1251.

[31] Induced nucleation of diamond powder. Frenklach, M, et al. 1991, Vol. 59, pp. 546-548.

[32] Fabrication of diamond nanopowder using microwave plasma torch technique. Ting, Chen-Ching, Young, Tai-Fa and Jwo, Ching-Song. 2007, Vol. 34, pp. 316-322.

[33] Formation of nanodiamonds at near-ambient conditions via microplasma dissociation of ethanol vapour. Kumar, Ajay, et al. 1-8, 2013, Nature Communications, Vol. 4.

[34] Shafraniuk, Serhii. Graphene: Fundamentals, Devices, and Applications. s.l. : Pan Stanford Publishing, 2015.

[35] A roadmap for graphene. Novoselov, K. S., et al. 2012, Nature, Vol. 490.

[36] Heteroatom-doped graphene materials: syntheses, properties and applications. Wang, Xuewan, et al. 2014, Chem. Soc. Rev., Vol. 43, pp. 7067-7098.

[37] Nitrogen-doped graphene films from chemical vapor deposition of pyridine: Influence of process parameters on the electrical and optical properties. Capasso, Andrea, et al. 2015, Beilstein Journal of Nanotechnology, Vol. 6, pp. 2028-2038.

[38] Pyridinic N doped graphene: Synthesis, electronic structure, and electrocatalytic property. Luo, Zhiqiang, et al. 2011, Journal of Materials Chemistry, Vol. 21, pp. 8038-8044.

[39] Synthesis of nitrogen-doped graphene films for lithium battery application. Reddy, Arava Leela Mohana, et al. 2010, ACS Nano, Vol. 4, pp. 6337-6342.

[40] Nitrogen-doped graphene: Synthesis, characterizations and energy applications. Xu, Haifeng, Ma, Lianbo and Jin, Zhong. 2018, Journal of Energy Chemistry, Vol. 27, pp. 146-160.

[41] Toward N-doped graphene via solvothermal synthesis. Deng, Dehui, et al. 2011, Chemistry of Materials, Vol. 23, pp. 1188-1193.

[42] Large scale synthesis of N-doped multi-layered graphene sheets by simple arc-discharge method. Li, Nan, et al. 2009, Carbon, Vol. 48, pp. 255-259.

[43] Nitrogen doped graphene via thermal treatment of composite solid precursors as a high performance supercapacitor. Haque, Enamul, et al. 2015, RSC Advances, Vol. 5, pp. 30679-30686.

[44] High graphite N content in nitrogen-doped graphene as an efficient metal-free catalyst for reduction of nitroarenes in water. Yang, Fan, et al. 2016, Green Chemistry, Vol. 18, pp. 4254-4262.

[45] Nitrogen-doped graphene for high-performance ultracapacitors and the importance of nitrogen-doped sites at basal planes. Jeong, Hyung Mo, et al. 2011, Nano Letters, Vol. 11, pp. 2472-2477.

[46] Production of N-graphene by microwave N2-Ar plasma. Dias, A., et al. 2016, Journal of Physics D: Applied Physics, Vol. 49, p. 55307.

[47] D Tsyganov et al 2016 Plasma Sources Sci. Technol. 25 015013, Tatarova 2018.

[48] Towards large-scale in free-standing graphene and N-graphene sheets. Tatarova, E. et al. 2017, Nature, Vol. 7.

[49] Silva, L. (2018). Microwave Plasmas Applied for Synthesis of Advanced Free-Standing Carbon Nanostructures (master dissertation).

[50] A tutorial discussion on measurements of rotational temperature in inductively coupled plasmas. Ishii, Izumi and Montaser, Akbar. 1991, Spectrochimica Acta Part B: Atomic Spectroscopy, Vol. 46, pp. 1197-1206.

[51] Microwave plasma torches driven by surface waves. Tatarova, E., et al. 2008, Plasma Sources Science and Technology, Vol. 17.

[52] Hexagonal Diamond—A New Form of Carbon. Bundy, F P and Kasper, J S. 1967, The Journal of Chemical Physics, Vol. 3437.

[53] On the n-diamond and i-carbon nanocrystalline forms. Bucknum, Michael J and Castro, Eduardo A. 2012, Vol. 50, pp. 1034-1038.

[54] Characterizing Graphene, Graphite, and Carbon Nanotubes by Raman Spectroscopy. Dresselhaus, M. S., Jorio, A. and Saito, R. 2010, Annual Reviews of Condensed Matter Physics, Vol. 1.

[55] Carbon structure in nanodiamonds elucidated from Raman spectroscopy. Korepanov, Vitaly I., et al. 2017, Carbon, Vol. 121, pp. 322-329.